HIGH SCHOOL EDITION
Journal of Student Research
Volume 13 Issue 4 (2024)

Neural Biomarker-Based Diagnosis of Alzheimer's Disease: AI Models and Electroencephalography

Shrey Kumar[1] and Jerry Zupan[#]

[1]Horace Greeley High School, USA
[#]Advisor

ABSTRACT

Millions of people in the United States suffer from Alzheimer's Disease (AD), an incurable form of dementia that continues to increase in prevalence. Current methods of AD diagnosis are limited to a late stage by which time the treatment options are limited, quality of life is poor, and cost of treatment is exponentially high. Early medical diagnosis of AD is difficult since standard non-invasive techniques require extensive tests and can still generate false positives and negatives, leading to misdiagnosis. This study proposes a supervised machine learning model trained on readily available Electroencephalography (EEG) patient data to diagnose potential AD patients. Relevant features were extracted and analyzed from an open-source EEG database, collected from 186 patients using the trained machine learning model of best fit. Our artificial intelligence (AI) model is an alternative to current late-state detection methods which require complex and risky procedures that can lead to inaccuracies. In addition, current algorithms require feature manipulation and sort through hundreds of thousands of raw EEG data points to obtain unreliable results. The results demonstrate that, given EEG data of 93 close-eyed patients, the trained logistic regression model- the machine learning model of best fit - achieved a sensitivity of 100% and overall accuracy of 87%, using data recordings of only eight second segments for each patient. This novel AD screening tool, with a cloud-based AI model, can be easily deployed at primary health care clinics tor screen patients for AD during their yearly clinical visits to increase early diagnosis.

Introduction

Rationale

Alzheimer's Disease (AD) is a brain related disorder that affects cognitive abilities including memory, focus, attention, visual perception, reasoning, judgement and comprehension (National Institute on Aging, 2023). The disease impacts 6.5 million Americans, with 121,499 officially dying from AD in 2019 (Alzheimer's Association, 2022). Total payments in 2022 for health care, long-term care and hospice services for people aged 65 and older with AD and related dementias are estimated to be $321 billion (Alzheimer's Association, 2022). The majority of spending is on long term care (~50%), but other care costs include Hospice (~10%) Medical facilities (~5%), Decedent's home (~30%), and several other costs (Alzheimer's Association, 2022). Figure 1 shows the progression of Alzheimer's Disease: AD moves from the medial temporal lobe, spreads to the lateral and parietal lobes, moves forward to the frontal cortex, and finally the occipital lobe. In each instance, the effects become more pronounced, affecting basic human functions like movement and sight (Alzheimer's Disease Fact Sheet, 2023).

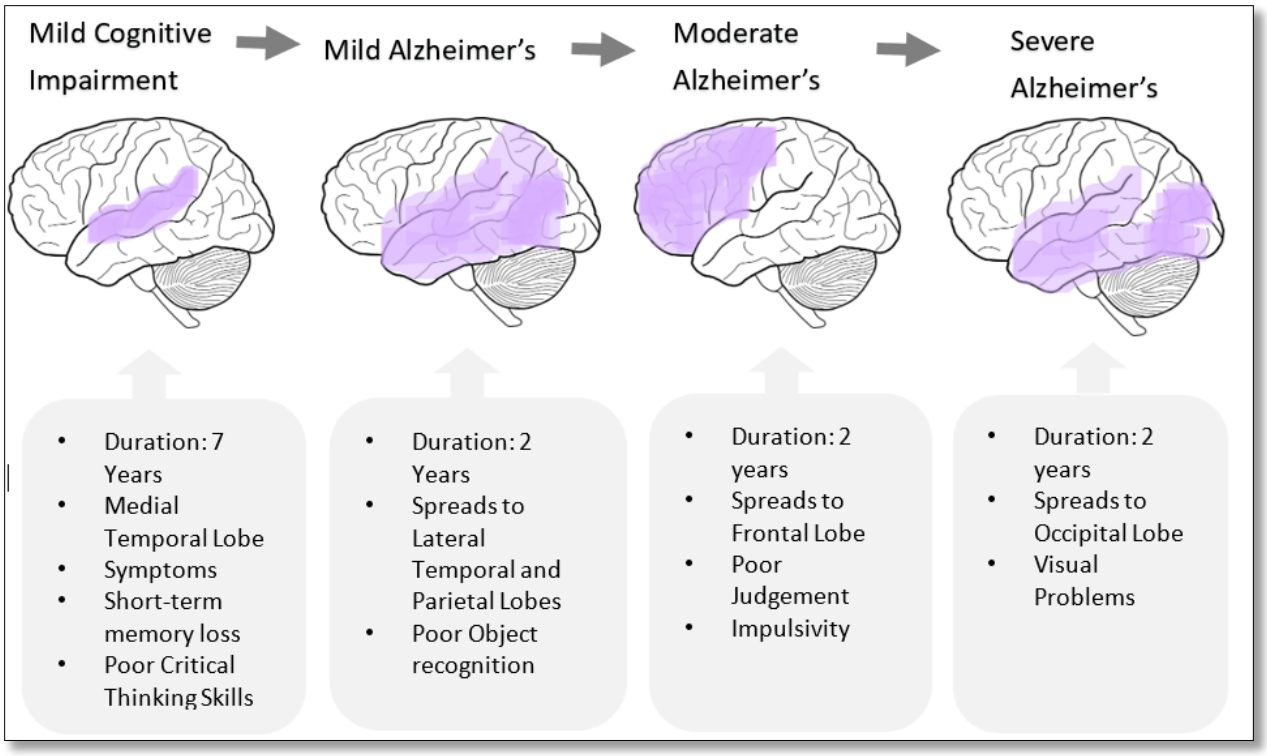

Figure 1. Schematic of the progression of Alzheimer's Disease in specific regions of the brain, and the effects over the span of several years.

The diagnosis of AD in its early stages can be used to determine effective therapeutic treatments that slow the effects of the disease (How Is Alzheimer's Disease Treated?, 2023). However, early medical diagnosis of Alzheimer's is difficult since standard non-invasive techniques require extensive tests and can still generate false positives, leading to misdiagnosis (Beach et al., 2012; Houmani et al., 2018). This study proposes a novel tool for low cost and high accuracy screening for AD using data from Electroencephalography (EEG) analyzed by a pre-trained supervised learning AI model. By using a readily available and clinically proven (FDA approved) data collection tool with cloud-based AI model, the proposed tool would aid in effectively screening every adult high-risk patient and support the goal of early detection and intervention of AD to improve disease outcomes.

Diagnostic Methods for AD

Current methods of AD diagnosis involve looking at the main pathological factors of AD, which include the deposition of the biomarker amyloid β in the brain (Murphy & LeVine, 2010). This can be measured by positron emission tomography (PET; illustrated in Figure 4) imaging, which observes blood flow, neurotransmitters, metabolism, and radiolabeled drugs (Wong et al., 2003). However, issues with radiologist training and interpretation exist: there can be up to 65% discrepancy in interpretation of PET imaging and the consensus diagnosis (Shipley et al., 2013). In other cases, neurologists use brief screening instruments such as the mini-mental state examination score and the Montreal cognitive test to assess patients, which function on a scale 0-30 to determine the type and severity of dementia (Trzepacz et al., 2015). Another method for AD diagnosis looks for signs of neuronal degeneration in the brain caused by the protein called tau phosphorylation. This is measured through the current gold standard for diagnosing AD, which is cerebrospinal fluid examination (CSF; Paraskevas & Kapaki, 2021). In a previous study the incidence of change in diagnosis resulting from CSF testing ranged from 7% to 27%, with the majority being a change from Mild

Cognitive Impairment (MCI) or non-AD to a diagnosis of AD. There were 8.5% and 10.3% changed diagnoses from AD to non-AD or MCI (Shaw et al., 2018). As such, there is a growing demand for the development of new, noninvasive approaches to aid in the early diagnosis of AD.

Electroencephalogram (EEG) Data

An electroencephalogram (EEG) is a non-invasive, low-cost medical device that captures the brain's electrical activity. The EEG uses small electrodes placed over the scalp to measure the absolute electrical potentials generated by the pyramidal neurons of the underlying cerebral cortex (Figure 2). The EEG headset first captures the brain's electrical field over certain regions using small electrodes. The electrical activity is small, so an amplifier then increases the signal so it can be converted into data points. These points mark the voltage of the EEG signal for an electrode at a specific time. Thousands of these data points are captured and then graphed to create a visualization of raw EEG waves (Figure 2). An estimated cortical area of 10 cm^2 discharging synchronously is required to generate a deflection on the scalp. When neurotransmitters are released at the endplate, excitatory or inhibitory postsynaptic potentials (EPSP/IPSP) are generated. The summation of EPSPs and IPSPs over a particular cortical region with large synchronous discharge creates an electrical field (neural activity) that the EEG can measure (Rayi et al., 2021).

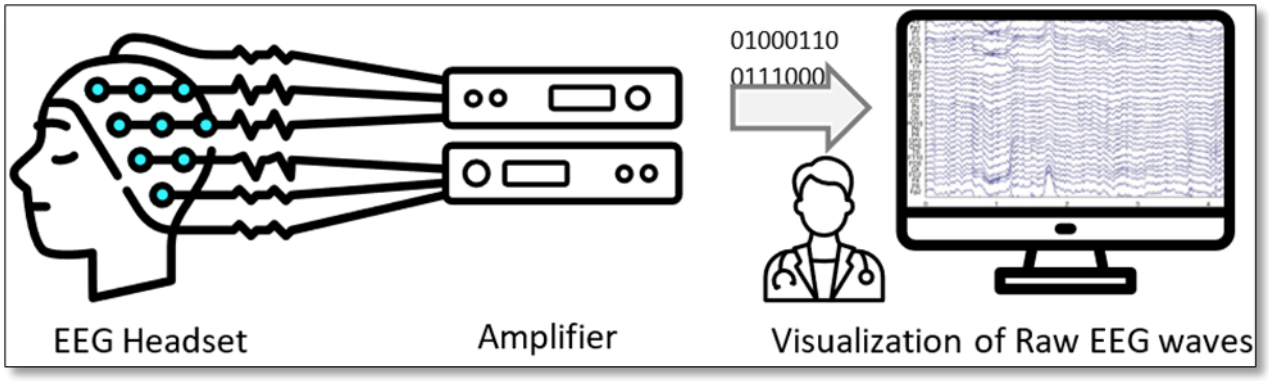

Figure 2. Illustration of the process by which neuron activity is converted into readable EEG signals on a computer. During resting or relaxed states, the EEG records a sinusoidal rhythmic activity called the posterior dominant rhythm (PDR) that is believed to result from oscillatory interaction between the visual cortex and the subcortical structures. During physical/mental activity, the cortical activity desynchronizes, and oscillatory activity replaces faster frequency and lower amplitude activity (Rayi & Murr, 2021).

Waveform frequencies in an EEG vary, including delta (0.5-4 Hz), theta (4-8 Hz), alpha (8-12 Hz), beta (12-30 Hz) and gamma (30-100 Hz) frequencies. Many studies show that EEGs have advantages in the simple collection, objective recording, and quantification of common waveform frequencies, making it suitable for the analysis of mental diseases (Nayak & Anilkumar, 2019).

Previous Diagnostic Uses of EEG Data

The electroencephalogram has previously been used to diagnose and treat several brain disorders. For example, Mild traumatic brain injury (mTBI) causes brain injury that results in electrophysiologic abnormalities visible on EEG recordings (O'Neil et al., 2011). Immediately after mTBI, there is epileptiform activity (high amplitude sharp waves or high frequency discharges), followed by suppression of cortical activity typically lasting 1–2 min, and followed by diffuse slowing of the EEG, which returns to the normal baseline within 10 min to one hour. qEEG most commonly shows immediate reduction in mean alpha frequency, with increased theta, increased delta, or increased theta:alpha

ratio (Ianof & Anghinah, 2017). Similarly, sleep disorders cause significant decreases in electric activity, specifically in the bilateral dorsolateral prefrontal cortex. As described in one study, the regional brain activity alteration in healthy subjects after a total of 36 h of sleep deprivation relative to after normal sleep, using a percent amplitude of fluctuation (PerAF) method. They found that sleep deprivation resulted in a 2.23% decrease in accuracy and an 8.82% increase in reaction time (Dai et al., 2021). Finally, the EEG is utilized to measure electrical disturbances in the human brain for the diagnosis of epileptic seizures. The normal shape of EEG signals gets modified during an epileptic seizure: many electrical disturbances start happening in the cerebrum of epileptic patients before a seizure's actual onset, which is termed a preictal stage (Shoka et al., 2023). An EEG can categorize these readings making it a useful tool when determining the type and onset of epilepsy (Ein Shoka et al., 2023).

Alzheimer's Detection Using EEG

Recent evidence suggests that synapse deficiency indicates AD in early cognitive decline (Subramanian et al., 2020). An EEG can detect this biomarker by observing the reduction in complexity of EEG signals, the increase/decrease in certain frequency bands, and changes in EEG synchrony (Houmani et al., 2018). Spectral analysis studies suggest that early stages of AD involve increased activity in the delta and theta frequency bands and a reduction in activity in the alpha and beta frequency bands (Lizio et al., 2011). Also, reduced spectral coherence - the relation in EEG signals - between the brain's two hemispheres for the alpha and beta frequency bands can indicate AD (Lizio et al., 2011). As Alzheimer's disease progresses in patients, alpha rhythms can transform, moving towards the anterior areas instead of remaining evenly distributed in the brain (Smailovic & Jelic, 2019). Therefore, biomarkers of AD are evident in the brain, yet to date there has been few accurate methods of analyzing EEG data for early diagnosis.

A Novel Machine Learning Model for AD Diagnosis

A promising method of analyzing EEG data associated with AD is using machine learning algorithms. By doing so, the screening time and human intervention are reduced, which makes the diagnostic results more efficient and objective (Xia et al., 2023). Classical machine learning algorithms have previously been trained with EEG signals for classifying various mental disorders, but they usually require complex feature engineering (FE) and subsampling processes to select appropriate features from raw EEG data, which becomes time-consuming for researchers (Xia et al., 2023). The solution is a support vector machine (SVM), or a supervised machine learning model that uses classification algorithms for two-group classification. Supervised learning algorithms such as the SVM model are able to make more efficient use of EEG data and improve the robustness of the algorithm.

Study Objective

Alzheimer's is a significant and costly public health issue that is typically diagnosed only after severe symptoms appear in patients. Current methods of diagnosis are either invasive or require complex feature engineering and subsampling processes, which are difficult for researchers. EEG and machine learning have been utilized to detect disease and improve clinical outcomes but have not been tested for detection of AD. This paper evaluates a novel non-invasive and efficient approach to detection of AD using machine learning algorithms trained on EEG data. This approach offers an alternative to currently used invasive diagnostic methods that require expensive and invasive tests, complex and time-consuming data collection. We hypothesize that raw EEG data processed into frequency bands for the electrodes can be fed into Support Vector Machine Models and used to predict early AD.

Methods

Data Sources

This study was exempt from IRB review because no primary data were collected. The data used in this study (Table 1) is secondary data initially collected jointly by Dr. Dennis Duke and other researchers at Florida State University. The dataset consists of 24 healthy elderly, all being negative for any neurological or psychiatric disorder, and 160 probable AD patients (12 Close eyed Healthy, 12 Open eyed Healthy, 80 Closed eyed AD, 80 Open eyed AD) diagnosed through the National Institute of Neurological and Communicative Disorders and Stroke and the Alzheimer's Disease and Related Disorders Association (NINCDS-ADRDA), and Diagnostic and Statistical Manual of Mental Disorders (DSM)-III-R criteria (Vicchietti et al., 2023). In this study, we utilized data from the closed-eyed patients only, as there is reduced interference with the electrical signals due to less eye movement when patients undergo EEG with their eyes closed (Barry et al., 2007).

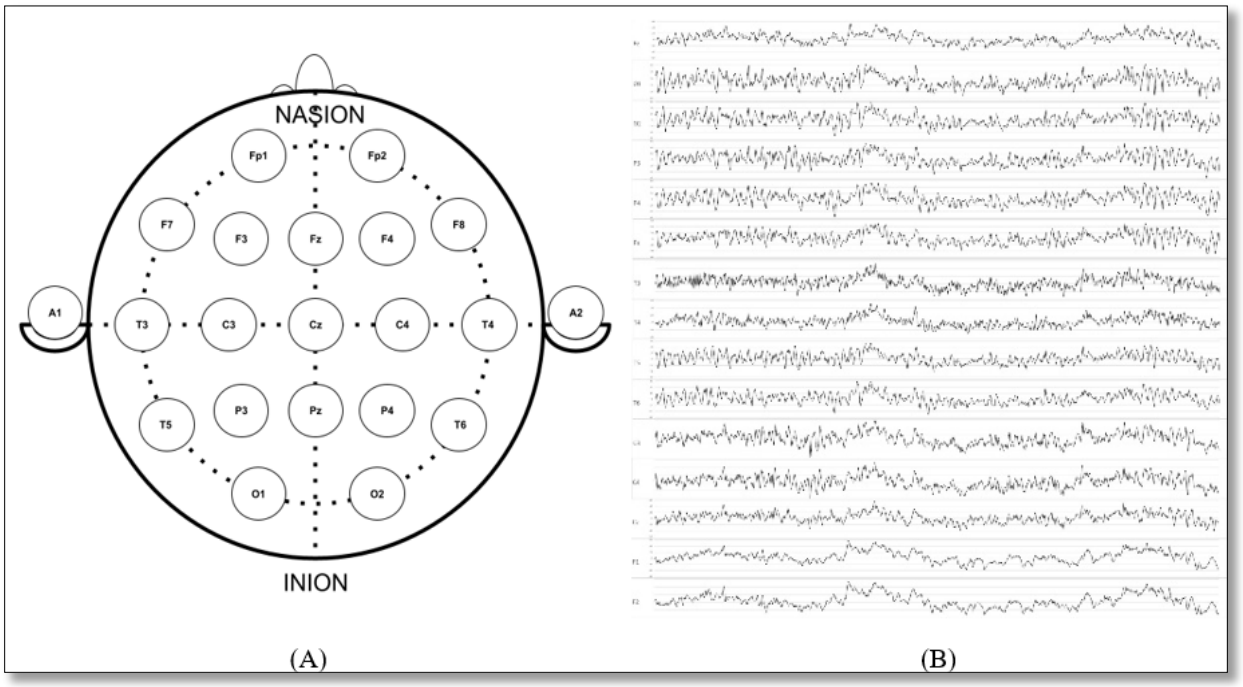

Figure 3. Schematic (A) shows the standard placement of 19 scalp electrodes in a 10-20 EEG system and the graph (B) is a demonstration of the plot for raw EEG data from Healthy Patient 1 with eyes closed for 15/19 electrodes.

The 10-20 system is an internationally recognized method that ensures electrode-spacing is 10-20% of the entire skull based on size and shape, starting from the nasion (indent between the forehead and nose) and ending at the inion (ridge at the base of the skull), as shown in Figure 3A. The electrodes comprise of Fp1, Fp2, F7, F3, Fz, F4, F8, T3, C3, Cz, C4, T4, T5, P3, Pz, P4, T6, O1, and O2 electrodes. Two reference electrodes are also used (A1 and A2) which cancel external interference between electrodes but will not be included in sample data as it is not significant to diagnosing AD. Numbers differentiate electrodes between the hemispheres, with even numbers (2, 4, 6, 8) corresponding to the right and odd (1, 3, 5, 7) referencing the left. Letters indicate the lobe, or area of the brain it is reading from and distance from the sagittal midline: pre-frontal (Fp), frontal (F), temporal (T), Parietal (P), Occipital (O), and Central (C) (Morley et al.). The data was taken from 19 scalp electrodes at a frequency of 128 Hz over an 8

second interval, generating 1024 EEG data points for each electrode. Using the Microsoft Excel software, the student created graphs for each electrode using a standardized scale in the original electrode placement, as shown in Figure 3B.

We used python programming language using Jupyter Notebook to develop the software. The code used in this study is publicly available in GitHub (GenerateEEGBands, 2024).

Approach to AD Detection

The methodology in this study uses a framework that consists of several steps. First, the raw EEG data referenced from the database (as described in Figure 4) is first collected as times-series data using EEG electrodes and imputed into a spreadsheet. The data is then pre-processed using a band pass filter, extracting frequencies from 1-55 Hz. The EEG data is then transformed into functionally distinct frequency bands by calculating power spectral density. Using visual analysis, frequency bands for electrodes with the highest discrimination are selected as relevant features, or the data used in training and testing the SVM models. The extracted relevant features for all AD and healthy patients were randomly partitioned into the training and test sets, with 80% of patients assigned to the training set and 20% allocated to the test set.

For the training set, patient data was processed by multiple SVM models. The SVM model of best fit (optimal decision boundary, detailed below) was then selected to classify the test data set to evaluate performance and fitting accuracy.

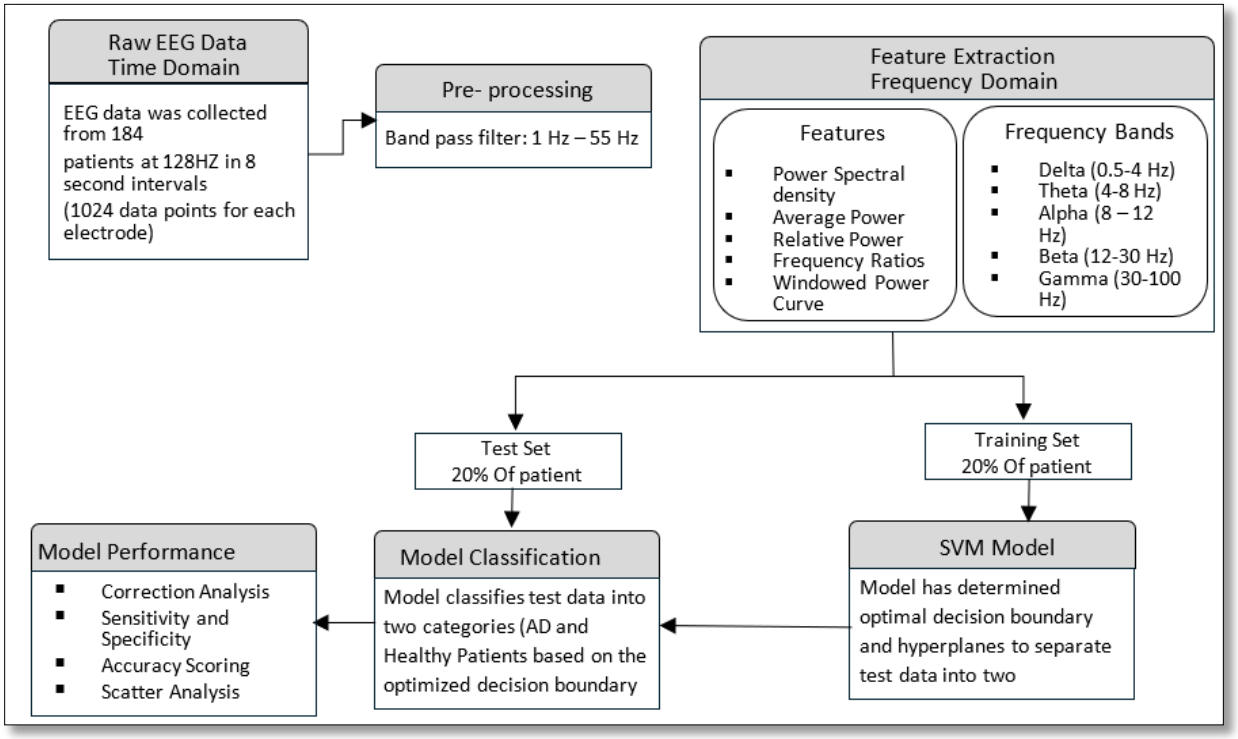

Figure 4. Flowchart of the overall modeling methodology for using EEG data to train the SVM models for the identification of potential AD patients.

EEG Data Preprocessing

The first preprocessing step was to transform the EEG data into functionally distinct frequency bands. Specifically, the goal was to compute delta (0.5–4 Hz), theta (4–8 Hz), alpha (8–12 Hz), beta (12–30 Hz), and gamma (30–100 Hz) bands in the dataset. Transforming the EEG signal into a specific frequency is performed using Fourier transformation. Fourier transformation is computed using an algorithm called Fast Fourier Transform (FFT). FFT returns for each frequency a complex number from which amplitude and phase of the signal is extracted for each specific frequency (delta, theta, alpha, beta, and gamma). Using spectral analysis, we obtain an estimate of power spectral density (or periodogram), expressed in (micro) Volts^2 per Hertz. For computation of spectral density, we used Welch's periodogram, which consists of averaging consecutive Fourier transforms of repeating signals. Figure 5 presents Welch's periodogram method used to create the power spectral density graph with the delta band highlighted in blue; taking the area of the blue polygon gives the absolute delta band power.

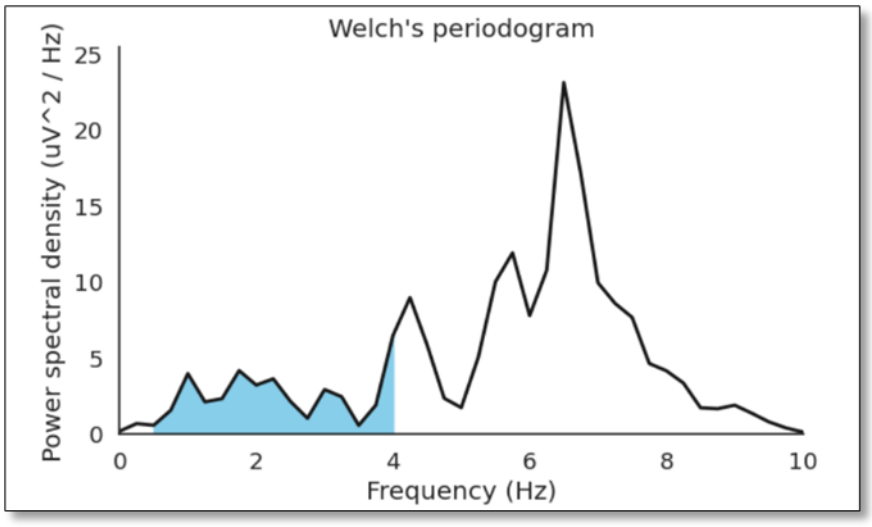

Figure 5. A plot of Welch's periodogram generated using Healthy Patient 1.

Table 1. Computation of all frequency band values for each electrode for one patient. The absolute power for each electrode across all frequency bands was calculated using Welch's periodogram method and formatted into the following table using Microsoft excel.

Electrode	Delta	Theta	Alpha	Beta	Gamma
C3	10.60438	18.96102	4.303051	2.343837	0.187688542
C4	8.79969	35.1022	5.063861	3.301477	0.177740901
Fp1	58.82602	23.81976	3.339879	2.487537	0.281819191
Fp2	63.02502	21.80444	3.800342	2.789324	0.563115254
Fz	15.88843	43.10278	4.531778	2.48771	0.238718511
O1	4.759462	9.196415	1.64365	2.24095	0.359242107
O2	5.270102	12.50652	1.577749	1.44269	0.157068639
P3	9.856439	15.42819	3.265286	1.912792	0.150530815
P4	8.023648	34.55506	4.722734	3.345265	0.169045158
Pz	8.800163	20.83357	3.028051	2.253788	0.16707739

T3	5.759189	4.273629	1.52749	1.153995	0.215209603
T4	4.049661	14.0314	3.993013	3.964438	0.665867214
T5	6.965542	8.763141	1.805596	2.673532	0.446689169
T6	3.867188	13.73349	2.848124	1.541352	0.152235558
Cz	11.35414	33.78903	4.85109	5.35517	0.238467977
F1	58.82602	23.81976	3.339878	2.487537	0.281819191
F2	63.02502	21.80444	3.800342	2.789324	0.563115254
F3	16.04242	31.04796	3.606483	2.789324	0.563115254
F4	16.93092	34.96975	4.93558	2.70223	0.398785732
F7	18.62485	16.72697	2.429497	1.77836	0.252503591
F8	24.63161	18.7295	3.827632	2.350093	0.357839136

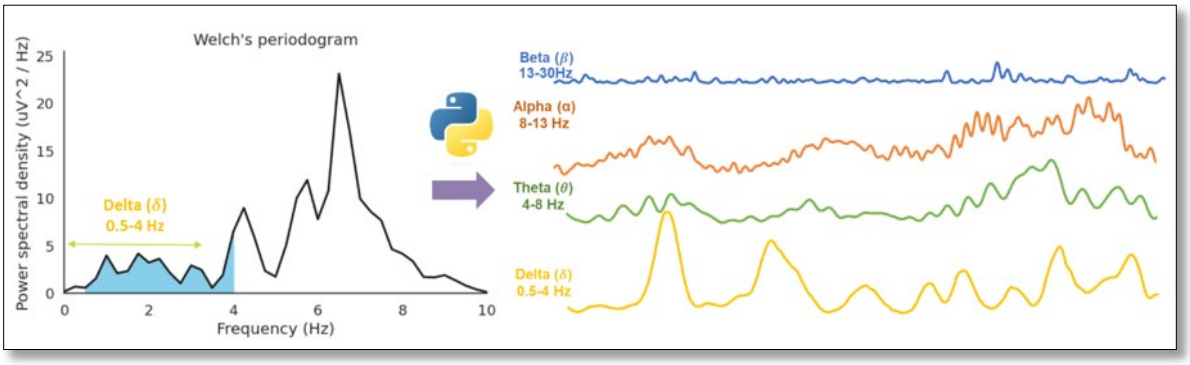

Figure 6. Decomposed EEG absolute band power of a healthy patient into windowed frequency components to calculate (Δ, Ø, ß, and α) for an 8 second interval data. The size of the frequency window was higher for lower band frequencies (Δ = 100) and lower for higher bands (ß = 20).

EEG Feature Extraction

The feature extraction was performed on all 19 electrodes, for 80 AD patients and 12 Healthy individuals with eyes closed. A subset of electrodes was selected based on t-tests and resulting p-values, showing statistical differences in the delta and theta frequency values between AD and healthy patients. Although we started with the subset of electrodes to develop and test the models, the software was evaluated on all 19 electrodes to collect the accuracy metrics as shown in the Expected Results section.

After pre-processing and spectral analysis of the various frequency bands, the Cerebral cortex electrodes (C3) were used since they produced the greatest average discrimination between AD and healthy patients. T-Test done on Delta frequency band values for AD and Healthy patients produced t test value of 3.49275 and p-value of 0.000746 indicating statistically significant difference. Among all frequency bands in C3, delta and theta had the highest discrimination rates (Figure 7). Therefore, in the trial, we took the absolute power for theta and delta frequency bands (measured in (micro)-Volts^2 per Hertz) for the C3 electrode with 70 AD patients and 7 healthy individuals randomly selected from the dataset for model development and training. The remaining 10 AD and 5 Healthy patient individuals were kept aside for model testing.

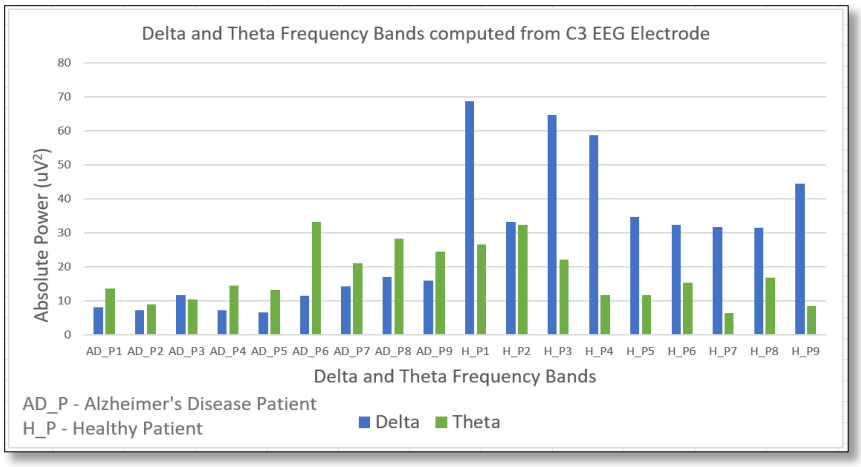

Figure 7. Comparison of the absolute powers (measured in uV^2) of the Delta and Theta frequency bands for Healthy and AD patients in the referenced study. As demonstrated, there is a clear difference in the absolute Delta power between AD and healthy patients.

To analyze brain waves, we used spectral estimation as a quantitative means of breaking down the EEG signal in terms of the different frequency waves that make it up, and their oscillatory power. We used the C3 electrode data to plot a spectral power at each time during the epoch.

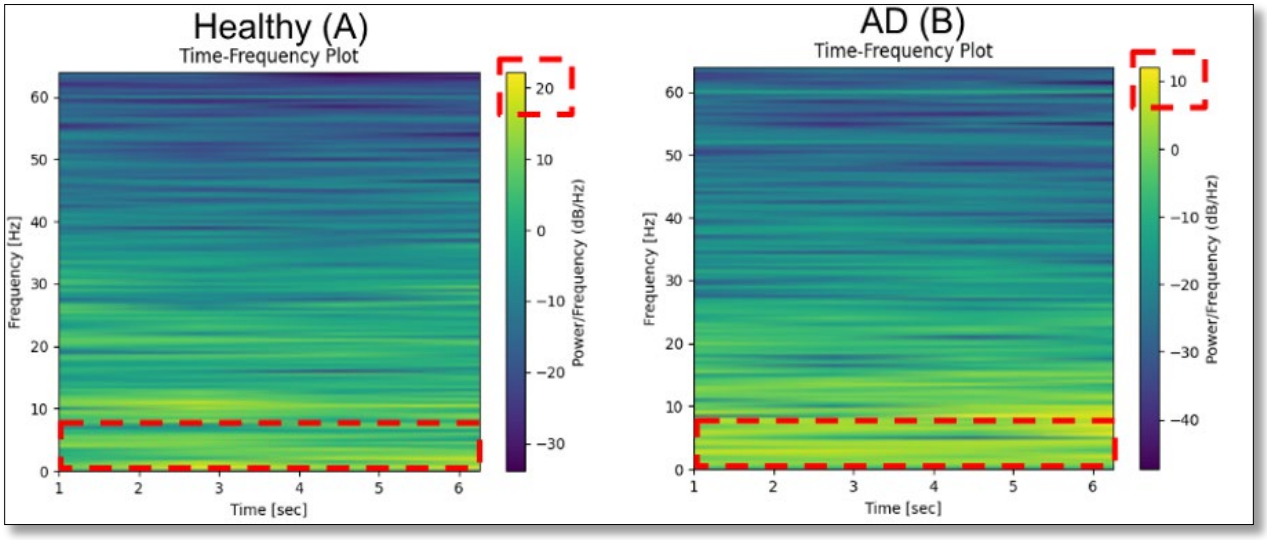

Figure 8. Time-frequency plot for C3 electrode, using Healthy Patient 1 (a) and AD Patient 1 (b), both with eyes-closed. Note that Healthy Patient 1 has a higher power frequency for Delta and Theta frequency bands than AD Patient 1 (according to the Power/Frequency legend, where Healthy Patient goes up to 20 dB/Hz vs. AD patient only goes up to 10 dB/Hz)

To do a spectral estimation of the brainwave, which is a non-stationary signal, we used the spectrogram to transform the brain waves into a time-frequency domain. The spectrogram in Figure 8 shows the frequency time plot, for a healthy and an AD patient, both with eyes closed. The x-axis represents the time in seconds, and the y-axis represents the frequency in Hertz. The legend shows the distribution of Power/Frequency in dB/Hz, with the color in

the graph corresponding to the power. The lighter color represents higher power. Because the code was written in python, the graphs generated are based on different Power/Frequency values, as shown in the legends. Note that the Healthy patient is on the (-30,20) Power/Frequency range, while the AD patient is on the (-40,10) Power/Frequency range, indicating the marked differences in Delta and Theta frequency bands.

SVM Model Development and Training

The model development was done on Jupyter Notebook using python programming and the SKlearn machine learning kit. First, the 80% of patients (77 patients, 70 AD + 7 Healthy) in the referenced study are imported and initialized in the Jupyter Notebook. This will be the training set, which comprises a vector of delta and theta absolute power for the training patients. Second, a vector of values (indicating 0=AD and 1=Healthy) corresponding to each tuple in the previous vector. This input data is given to 5 models, namely the DecisionTreeClassifier, KNeighborsClassifier, SVC, Logistic Regression, and VotingClassifier. Since an SVM is a supervised learning model, it takes into account the vector of values (patient's diagnosis) to estimate a line that most accurately discriminates between AD and Healthy patients, known as a decision boundary.

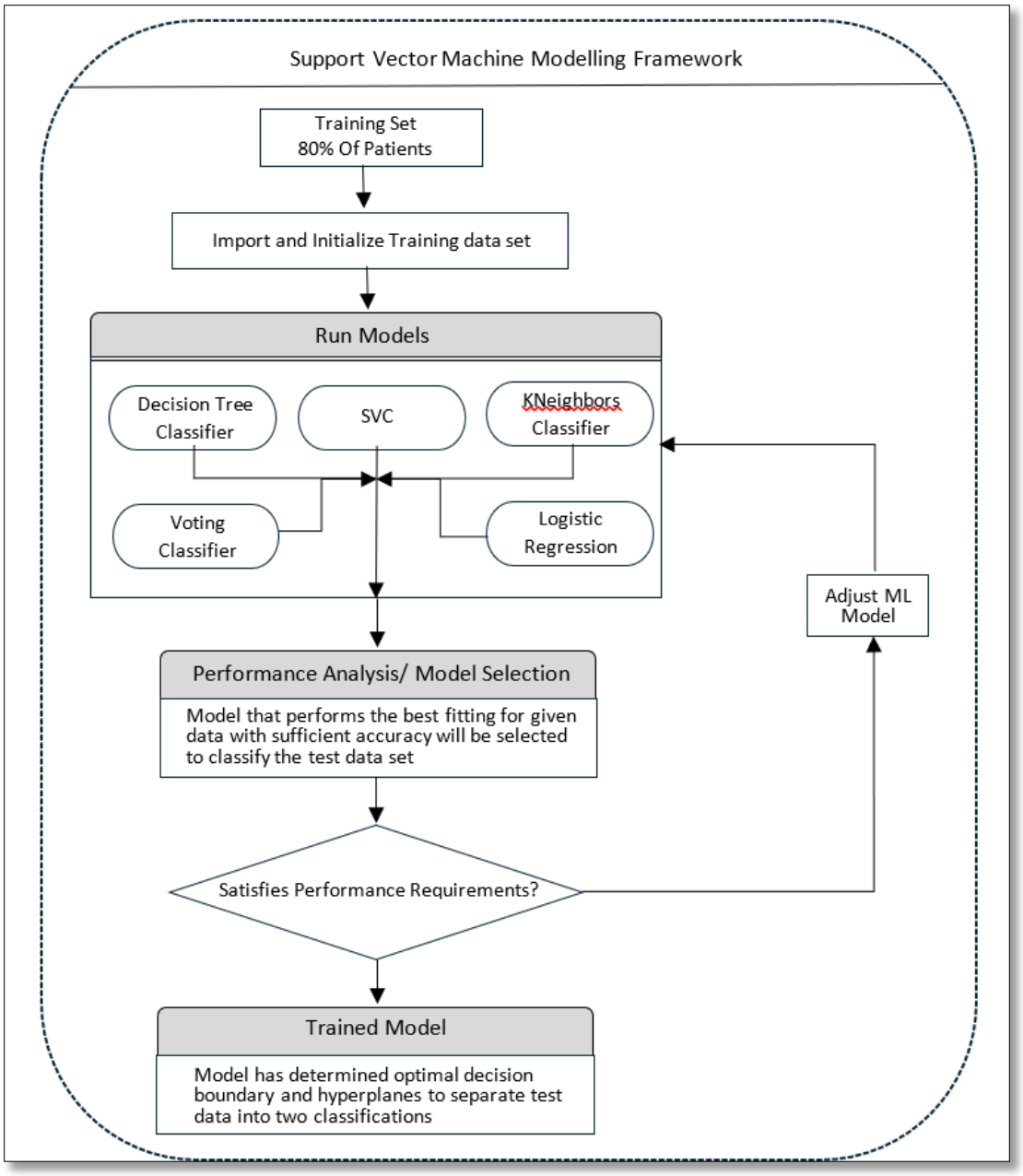

Figure 9. Flowchart depicting the workflow for training and adjusting the SVM models.

SVM Model Selection and Scoring

Using the framework presented in Figure 11, each model was trained on the data. This consisted of using the vector of patient values (indicating 0=AD and 1=Healthy) to create a decision boundary to classify a patient with a certain absolute theta and delta powers as either AD or healthy. A statistical analysis was performed using the t-test to compute the p-values for AD and Health patients for the delta band. After each SVM model generated a distinct decision boundary based on the method of classification, we observed the hyperplanes created to determine which model had the clearest boundary with the given data set. This model will then be selected to classify the test data since it proved to be the SVM model with the highest classification accuracy.

Expected Results

We expect the machine learning trained model will give an estimation of statistical significance whether SVM models trained on EEG data can be used to identify patients, namely AD vs. Healthy. In order to test the reliability and validity of our mode, we use six statistical measures, namely Sensitivity (recall), Precision, F1 Score, Accuracy, and Sensitivity. The calculation of each of the measures is done using a confusion matrix (Table 2).

Table 2. Two by two table with corresponding formulas for recall (RC), precision (PC), F1 score and accuracy.

Confusion Matrix		
		Predicted Values
Actual Values	Positive	Negative
	True Positive (TP)	False Negative (FN)
	False Positive (FP)	True Negative (TN)

Recall (RC): measures how often a machine learning model correctly identifies positive instances (true positives) from all the actual positive samples in the dataset.

$$Recall\ (RC) = \frac{TP}{(TP + FN)}$$

F1 Score: The harmonic mean of a classification model's precision and recall.

$$F1\ Score = 2 * \frac{PC * RC}{(TP + FP)}$$

Precision (PC): The accuracy of positive predictions (measures how many of all positive cases detected were true positives)

$$Precision\ (PC) = \frac{TP}{(TP + FP)}$$

Accuracy: Measures how often a machine learning model correctly predicts the outcome, whether classifying a positive or negative case

$$Accuracy = \frac{TP + TN}{(TP + TN + FP + FN)}$$

Our goal is to focus more on sensitivity of the model (recall / true positive rate / hit rate) which refers to the ability of the model to identify AD patients. We want to calculate the precision which measures the ratio of correctly identified AD patients over the total number of actual AD patients. We also calculated F1 Score which is the weighted average of precision and recall. Finally, we want to compute the accuracy of the model which is the ratio of records that model identified correctly (AD and healthy) over the total record set.

Results

SVM Model Selection

In order to select the most accurate model, the absolute power for each electrode across the complete dataset (AD = 80 and Healthy =12) was created as a comma separated file (csv). Since each model requires data formatted in an x and y variable (for plotting), we took the calculated absolute delta and theta powers for each patient to input into a csv file. The data was then ingested by the python code for first training the model. We used several python packages in Jupyter Notebook, such as NumPy, SciPy, CSV, and Seaborn. In the program, we created separate testing and testing files to separate the respective patient pools. Using the SKlearn package for the machine learning models, the files were inputted into the program, creating a plot of the five models.

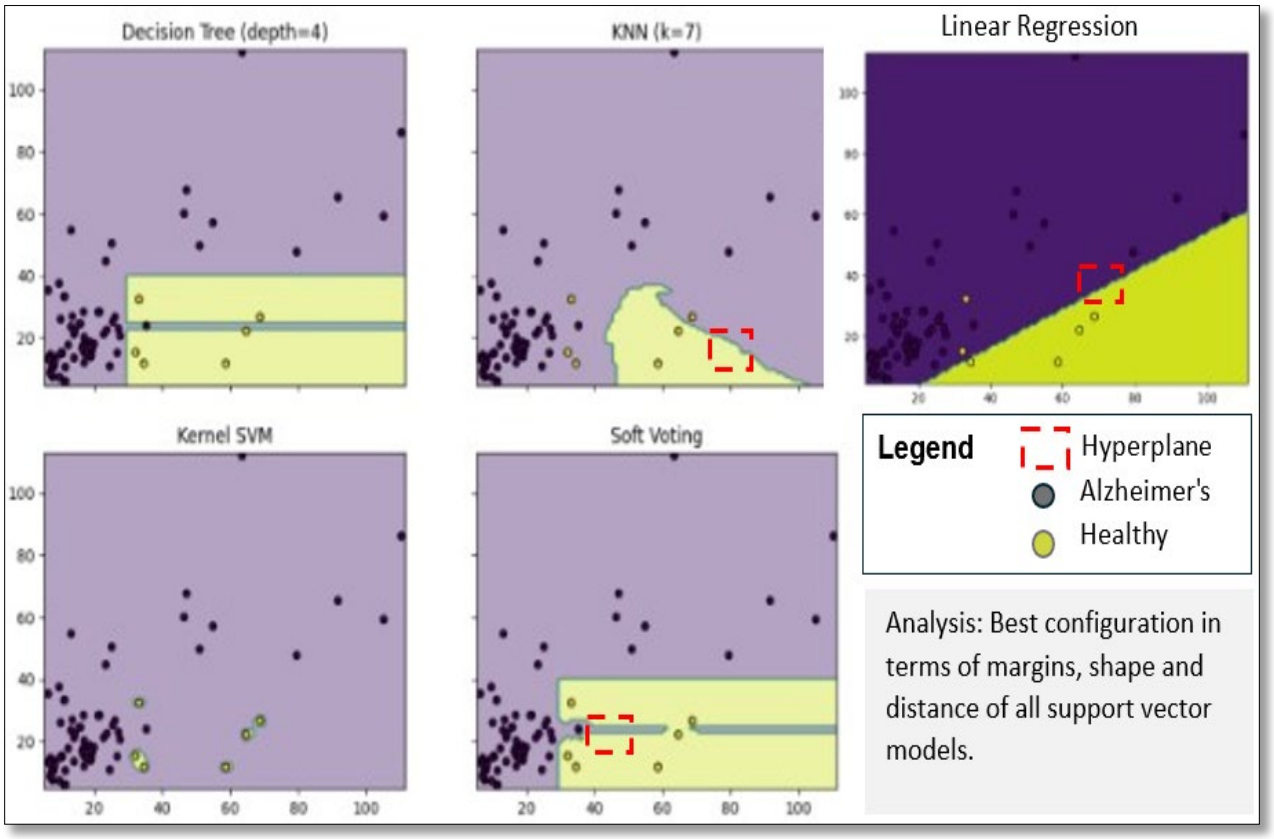

Figure 10. Results of training the model on a 2-dimensional feature space using the C3 electrode for healthy (hollow dots) and Alzheimer's (black dots) patients. The hyperplane separates the two clusters, and the X and Y axis represent the delta and theta values respectively.

Each trained model also produced a scatter plot (Figure 10) that gives a visual representation of the trained models hyperplane. The visual analysis of the hyperplane provided insights into the stability of the model. In figure 10, models such as the Kernel SVM highlight the instances of patients having Alzheimer's, while leaving the rest of the plot to classify healthy patients. This is considered an unstable model, as it does well in classifying the training set, but when applying the testing set or any other patient data, the model would struggle to classify many patients correctly as healthy, as many don't have the exact delta and theta powers. On the other hand, the Linear Regression model would be considered a stable model. This is because the hyperplane is a line, which is much more general than individually circling healthy patients. In addition, it also shows a clear discrimination between AD and healthy patient's absolute powers. All the 19-electrode's absolute power for the delta and theta frequency bands was processed

through the program for first creating the trained model and then running the corresponding electrode's scoring dataset for computation of statistical accuracy.

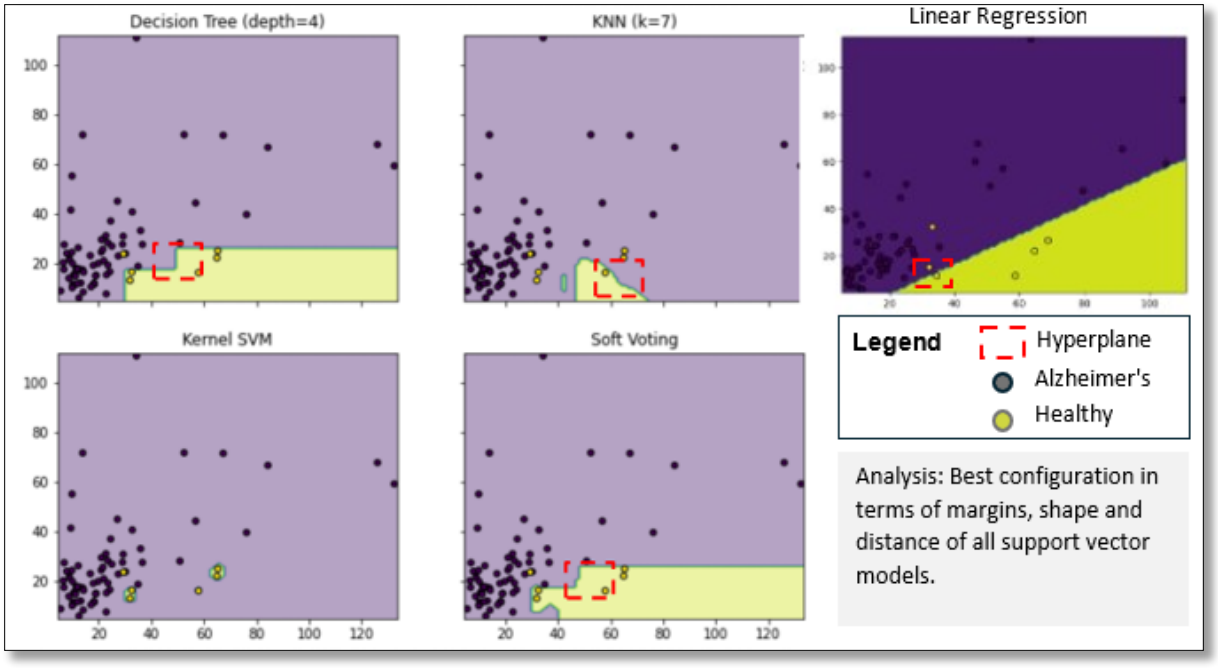

Figure 11. Results from the C4 electrode training the model on a 2-dimensional feature space showing that the linear regression model represents the hyperplane of best fit given the inputted patient data from healthy (hollow dots) and Alzheimer's (Black dots) patients

SVM Model Results

Among the SVM models used, the hyperplane created by the linear regression model proved to be the best fitting and the most stable for the given dataset (Figure 10 and 11). The linear regression trained models for each electrode were then fed the scoring dataset (AD = 10 and Healthy = 5) to produce the results of the scored model with 0 = AD and 1 = Healthy. Table 3 shows the results of the linear regression model run on 10 AD and 5 Healthy patients across all 19 electrodes. Patients AD_1, AD_2, AD_3, AD_4, AD_6, AD_7, AD_8, AD_9, and AD_10 was scored correctly across all electrodes. Only C3, C4, and F3 were able to correctly identify patient AD_5. For healthy patients, only C3, C4, and F4 consistently produced high accuracy, except for H_2, which was incorrectly forecasted for all electrodes.

Table 3. Results of linear regression model scoring across all 19 electrodes, for 10 AD and 5 Healthy patients.

Electrode	AD_1	AD_2	AD_3	AD_4	AD_5	AD_6	AD_7	AD_8	AD_9	AD_10	H_1	H_2	H_3	H_4	H_5
C3	0	0	0	0	1	0	0	0	0	0	1	0	1	1	0
C4	0	0	0	0	0	0	0	0	0	0	1	0	1	1	0
Cz	0	0	0	0	1	0	0	0	0	0	0	0	1	0	0
F1	0	0	0	0	0	0	0	0	0	0	0	0	1	0	0
F2	0	0	0	0	0	0	0	0	0	0	0	0	1	0	0
F3	0	0	0	0	1	0	0	0	0	0	1	0	1	1	0

F4	0	0	0	0	0	0	0	0	0	0	1	0	1	0	0
F7	0	0	0	0	0	0	0	0	0	0	0	0	1	0	0
F8	0	0	0	0	0	0	0	0	0	0	0	0	1	0	0
Fp1	0	0	0	0	0	0	0	0	0	0	0	0	1	0	0
Fp2	0	0	0	0	0	0	0	0	0	0	0	0	1	0	0
Fz	0	0	0	0	1	0	0	0	0	0	0	0	1	0	0
O1	0	0	0	0	0	0	0	0	0	0	0	0	0	0	0
O2	0	0	0	0	0	0	0	0	0	0	0	0	0	0	0
P3	0	0	0	0	0	0	0	0	0	0	0	0	0	0	0
P4	0	0	0	0	0	0	0	0	0	0	0	0	0	0	0
Pz	0	0	0	0	0	0	0	0	0	0	0	0	0	0	0
T3	0	0	0	0	0	0	0	0	0	0	0	0	1	1	0
T4	0	0	0	0	0	0	0	0	0	0	0	0	1	0	0
T5	0	0	0	0	0	0	0	0	0	0	0	0	0	0	0

Table 4 shows the summary statistics and accuracy calculations for all 19 electrodes, using the results from table 3. The first 4 columns correspond to the core statistical metrics, including True Positive (TP), True Negative (TN), False Positive (FP), and False Negative (FN). Using these raw metrics, we then calculated the Sensitivity, Specificity, Precision, F1 score, Accuracy, True Positive Rate (TPR), and False Positive Rate (FPR) in Microsoft Excel, using their respective equations. Table 4 depicts these results in percentage form, color coding the metrics based on the electrode's performance. Since all models performed relatively well in detecting AD cases (>90% sensitivity), the color coding was done based on specificity. Green means the model's specificity was >60%, yellow corresponds to >=20%, and red means that the model performed poorly with <20% specificity. As demonstrated, the C3, C4, and F3 electrodes performed the best, with overall high specificity metrics, while electrodes such as O1 and O2 performed poorly.

Table 4. Summary statistics and accuracy metrics computed for all 19 electrodes.

Electrode	TP	TN	FP	FN	Sensitivity	Specificity	Precision	F1 Score	Accuracy	TPR	FPR
C3	9	3	2	1	90%	60%	81.8%	86%	80%	90%	40%
C4	10	3	2	0	100%	60%	83.3%	91%	87%	100%	40%
Cz	9	1	4	1	90%	20%	69.2%	78%	67%	90%	80%
F1	10	1	4	0	100%	20%	71.4%	83%	73%	100%	80%
F2	10	1	4	0	100%	20%	71.4%	83%	73%	100%	80%
F3	9	3	1	1	90%	75%	90.0%	90%	86%	90%	25%
F4	10	2	3	0	100%	40%	76.9%	87%	80%	100%	60%
F7	10	1	4	0	100%	20%	71.4%	83%	73%	100%	80%
F8	10	1	4	0	100%	20%	71.4%	83%	73%	100%	80%
Fp1	10	1	4	0	100%	20%	71.4%	83%	73%	100%	80%
Fp2	10	1	4	0	100%	20%	71.4%	83%	73%	100%	80%
Fz	9	1	4	1	90%	20%	69.2%	78%	67%	90%	80%
O1	10	0	5	0	100%	0%	66.7%	80%	67%	100%	100%
O2	10	0	5	0	100%	0%	66.7%	80%	67%	100%	100%
P3	10	0	5	0	100%	0%	66.7%	80%	67%	100%	100%
P4	10	0	5	0	100%	0%	66.7%	80%	67%	100%	100%

Pz	10	0	5	0	100%	0%	66.7%	80%	67%	100%	100%
T3	10	2	3	0	100%	40%	76.9%	87%	80%	100%	60%
T4	10	1	4	0	100%	20%	71.4%	83%	73%	100%	80%
T5	10	0	5	0	100%	0%	66.7%	80%	67%	100%	100%
T6	10	0	5	0	100%	0%	66.7%	80%	67%	100%	100%

The results the 19 electrodes are summarized in figure 12, which shows the relative accuracies of each electrode depicted in the 10-20 EEG system. The color coding is based on the previously defined green, yellow, and red categorization of the specificity of the model. It is noteworthy that each of these three electrodes is located on the Central and Frontal lobe of the brain, which are the affected areas in cases of early to mild Alzheimer's disease.

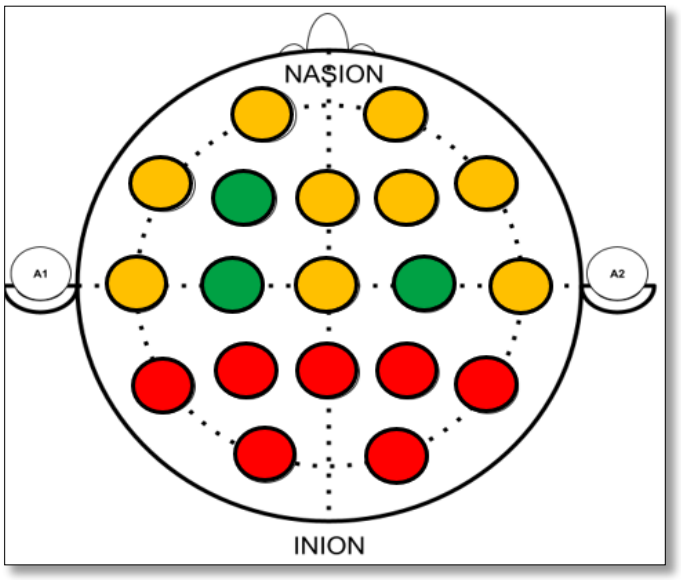

Figure 12. The figure shows the performance of each electrode, demonstrated on the EEG headset map.

The Receiver Operating Characteristic (ROC) plot is a graph as shown in figure 13 plots the performance of the linear regression model across all 19 electrodes. The X-axis shows the false positive rate (incorrectly classifying patients as AD), while the Y-axis shows the true positive rate (correctly classifying patients as AD). As demonstrated in ROC plot in figure 13, the C3, C4 and F3 electrodes had a false positive rate below 50%, which is considered an acceptable result. The other 16 electrodes had higher than acceptable false positive rates, with the highest being the O1 and O2 electrodes.

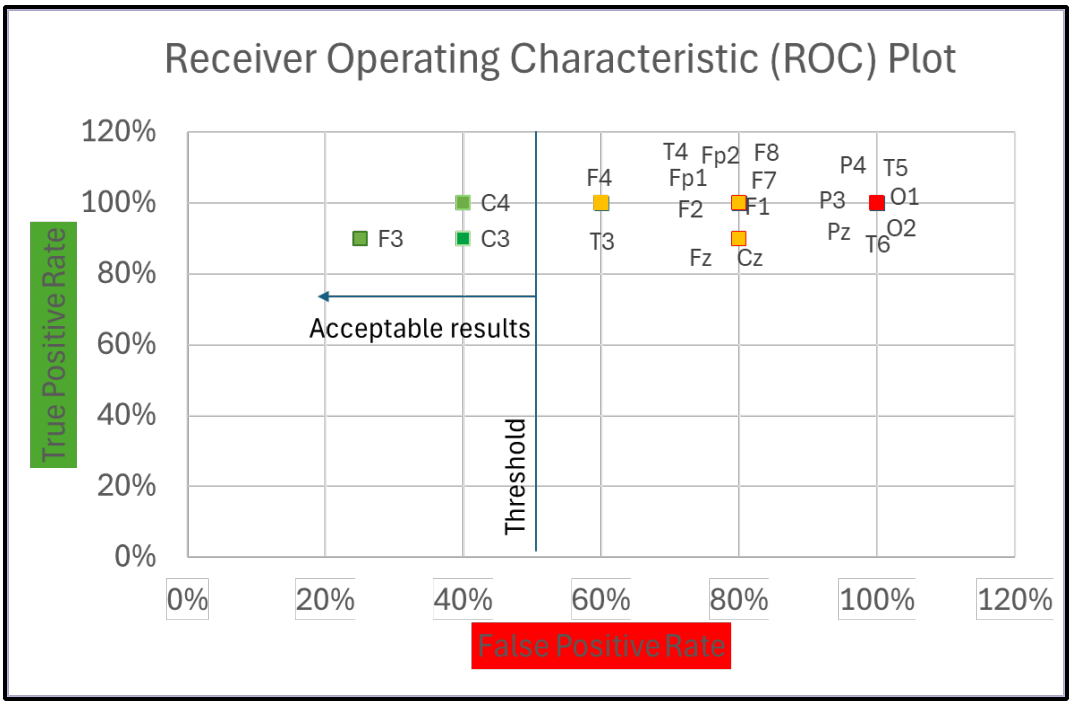

Figure 13. The figure shows the ROC plot for all 19 electrodes.

Table 5 shows the specific results for the best performing electrodes, including C3, C4, and F3. The classification table shows that on average, each electrode had 9-10 true positive cases and 2-3 true negative cases. False positives and negatives were a total of 3 on average. This means that for the best performing electrodes, the linear regression model had high performance in cases where the patient has AD, whereas it had a poor performance on the healthy patients, giving almost an equal number of false positives. This still averages to an overall high performance, as in the testing set, there is a greater number of AD than healthy. As stated previously, we calculated the four-accuracy metrics, which are shown in the performance table. Based on the >=90% recall (sensitivity) and >=60% specificity, these three electrodes were considered to have the highest performance. However, while each model achieved a high sensitivity, C4 had the highest overall accuracy in classifying patients with 87%.

Table 5. Results of contingency table analysis and linear regression for model performance using data from the C3 and C4 electrodes.

	Classification (N)				Performance (%)			
Electrode	TP	FN	FP	TN	Recall	Precision	Specificity	Accuracy
C3	9	1	2	3	90	81.8	60	80
C4	10	0	2	3	100	83.3	60	87
F3	10	0	3	2	90	90	75	86

Note: TP= true positive; FN= false negative; FP= false positive; TN= true negative; N= number observed of 15 and C4 electrodes.

Discussion

The results of our model training demonstrated that linear regression is the best fitting model with the given data. Hence, Logistic Regression was selected as the SVM model of choice for further scoring. From the SVM model's classification of the test data, it is clear that the statistical measures used to score the model demonstrate that SVM models trained on EEG data can reliably be used to identify patients, namely AD vs. Healthy.

In clinical practices, doctors must discriminate between patients suffering from Alzheimer's disease from patients with other types of dementia, cognitive impairment, or other conditions. AD is consequently difficult to diagnose and differentiate without the use of cerebrospinal fluid (CSF) biomarkers or single-photon emission computerized tomography (SPECT-scan).

Alzheimer's Disease detection today is limited to the late stage by which time the treatment options are limited, and quality of life is poor. Additionally, the misdiagnosis of Alzheimer's has become a costly issue. Patients with prior AD diagnosis use substantially more unsuitable medical services approximately $9,500 - $14,000 annually until their diagnosis of related dementias (Hunter et al., 2015). Making EEG-based early detection of AD useful, despite coming with some limitations. First, current diagnosis of Alzheimer's disease -either using invasive methods or EEG data - is conducted by researchers: data is analyzed using human interpretation, which is subject to human error and misdiagnosis. Second, most publications are based on relatively small databases, containing EEG data for approximately 20 people per study. Small sample sizes limit the accuracy of a supervised learning model such as the SVM since it is trained on data with little variation. Third, many studies are limited in the number of relevant features. EEG data needs to be taken from certain electrodes over a relevant frequency band to be fed into a supervised learning model rather than all EEG data collected, which limits the amount of data the model can be trained on and eliminates frequency bands which could potentially show signs of AD, since the disease has varying effects on individuals.

The present study overcomes such limitations and eliminates the need for human interpretation of EEG-data using a supervised learning model. Our research analyzes a bigger database of 93 patient EEG recordings, in real clinical conditions. The SVM model uses all EEG features extracted from patients for clinical diagnosis of AD. To the best of our knowledge, no study thus far has carried out AD diagnosis using an SVM model on a medium EEG database, considering all the given EEG features (of the 10-20 system).

The novel approach presented in the paper has potential limitations. We have developed the tool using only 80 AD and 12 Healthy patients. Also, the EEG data is limited to only eight seconds. The data limitation in this study impacts the ability of the model to assess its accuracy in a real-world setting. Also, the model will benefit from dimensionality analysis and reduction techniques like Principle Component Analysis (PCA) applied on all frequency bands (Δ, ∅, ß, and α) done across individual or sets of electrodes namely F: Frontal, C: Central, T: Temporal, P: Parietal; O: Occipital. Since for AD patients, the signals on left and right hemispheres can vary, PCA analysis can help identify the best set of frequency bands to be used in the model training (Greenacre et al., 2022).

Conclusion

The proposed approach in this paper offers advantages over the current clinical based diagnosis of Alzheimer's disease. Today, AD diagnosis is performed at late stages, limiting treatment options and effectiveness. There is no clinical screening option available for non-invasive and low-cost early-stage AD detection. Having AD screening available at primary care clinics during a person's yearly visit has the potential to transform the approach to AD diagnosis and treatment providing patients precious time to prepare for the monetary effects of AD and the effects on a person's ability to live independently

In our framework, we developed a simple two-step approach to AD screening. Step one involves collecting EEG data for a period of less than 2 minutes per patient. This data is then fed to a cloud-based AD identification system that uses a Support Vector Machine model pre-trained on historical AD patients. In less than 10 seconds, the

system predicted the likelihood of patients having AD symptoms. Using this real-time result, a clinician can perform further diagnosis using existing methods to help confirm the diagnosis and prescribe an optimized treatment plan. Although our initial study used a small set of data, nevertheless, it demonstrates the scalability, feasibility, and accuracy of using a machine learning model. The proposed novel approach to AD detection using Support Vector Machine Models applied to EEG data provided 90% sensitivity and 80% specificity. Since EEG is an FDA approved and low-cost device, electrode-based data collection tool, detecting patients' early stages of their AD can lead to intervention and more effective treatments.

In future work, we will use more candidate electrodes besides C3, which will provide more discriminatory factors between AD and healthy patients. Additionally, additionally training and testing the primary SVM model on patients with cognitive impairment or other pathologies, patients can be more accurately diagnosed and treated accordingly.

Acknowledgments

I would like to thank my advisor for the valuable insight provided to me on this topic.

References

1. Alzheimer's Association. (2022). 2022 Alzheimer's disease facts and figures. *Alzheimer's & Dementia*, *18*(4). https://doi.org/10.1002/alz.12638
2. Alzheimer's Association. (2023). *Facts and Figures*. Alzheimer's Disease and Dementia; Alzheimer's Association. https://www.alz.org/alzheimers-dementia/facts-figures
3. Barry, R. J., Clarke, A. R., Johnstone, S. J., Magee, C. A., & Rushby, J. A. (2007). EEG differences between eyes-closed and eyes-open resting conditions. *Clinical Neurophysiology: Official Journal of the International Federation of Clinical Neurophysiology*, *118*(12), 2765–2773. https://doi.org/10.1016/j.clinph.2007.07.028
4. Beach, T. G., Monsell, S. E., Phillips, L. E., & Kukull, W. (2012). Accuracy of the Clinical Diagnosis of Alzheimer Disease at National Institute on Aging Alzheimer Disease Centers, 2005–2010. *Journal of Neuropathology & Experimental Neurology*, *71*(4), 266–273. https://doi.org/10.1097/nen.0b013e31824b211b
5. Dai, X.-J., Zhang, J., Wang, Y., Ma, Y., & Shi, K. (2021). Editorial: EEG and fMRI for Sleep and Sleep Disorders–Mechanisms and Clinical Implications. *Frontiers in Neurology*, *12*. https://doi.org/10.3389/fneur.2021.749620
6. Ein Shoka, A. A., Dessouky, M. M., El-Sayed, A., & Hemdan, E. E.-D. (2023). EEG seizure detection: concepts, techniques, challenges, and future trends. *Multimedia Tools and Applications*. https://doi.org/10.1007/s11042-023-15052-2
7. Emmady, P. D., & Tadi, P. (2022). Major Neurocognitive Disorder (Dementia). *PubMed; StatPearls Publishing*. https://www.ncbi.nlm.nih.gov/books/NBK557444/
8. Greenacre, M., Groenen, P. J. F., Hastie, T., D'Enza, A. I., Markos, A., & Tuzhilina, E. (2022). Principal component analysis. *Nature Reviews Methods Primers*, 2(1), 1–21. https://doi.org/10.1038/s43586-022-00184-w
9. Houmani, N., Vialatte, F., Gallego-Jutglà, E., Dreyfus, G., Nguyen-Michel, V.-H., Mariani, J., & Kinugawa, K. (2018). Diagnosis of Alzheimer's disease with Electroencephalography in a differential framework. *PLOS ONE*, *13*(3), e0193607. https://doi.org/10.1371/journal.pone.0193607
10. How Is Alzheimer's Disease Treated? (2023). National Institute on Aging. https://www.nia.nih.gov/health/alzheimers-treatment/how-alzheimers-disease-treated

11. Hunter, C. A., Kirson, N. Y., Desai, U., Cummings, A. K. G., Faries, D. E., & Birnbaum, H. G. (2015). Medical costs of Alzheimer's disease misdiagnosis among US Medicare beneficiaries. *Alzheimer's & Dementia*, 11(8), 887–895. https://doi.org/10.1016/j.jalz.2015.06.1889
12. Ianof, J. N., & Anghinah, R. (2017). Traumatic brain injury: An EEG point of view. *Dementia & Neuropsychologia*, *11*(1), 3–5. https://doi.org/10.1590/1980-57642016dn11-010002
13. Jiao, B., Li, R., Zhou, H., Qing, K., Liu, H., Pan, H., Lei, Y., Fu, W., Wang, X., Xiao, X., Liu, X., Yang, Q., Liao, X., Zhou, Y., Fang, L., Dong, Y., Yang, Y., Jiang, H., Huang, S., & Shen, L. (2023). Neural biomarker diagnosis and prediction to mild cognitive impairment and Alzheimer's disease using EEG technology. *Alzheimer's Research & Therapy*, 15(1). https://doi.org/10.1186/s13195-023-01181-1
14. Johns Hopkins Medicine. (2019). *Electroencephalogram (EEG)*. John Hopkins Medicine. https://www.hopkinsmedicine.org/health/treatment-tests-and-therapies/electroencephalogram-eeg
15. GenerateEEGBands. GitHub. https://github.com/AlphaIsGoated/GenerateEEGBands
16. Lizio, R., Vecchio, F., Frisoni, G. B., Ferri, R., Rodriguez, G., & Babiloni, C. (2011). Electroencephalographic Rhythms in Alzheimer's Disease. *International Journal of Alzheimer's Disease*, 2011, 1–11. https://doi.org/10.4061/2011/927573
17. Mayo Clinic . (2018). *EEG (electroencephalogram) - Mayo Clinic*. Mayoclinic.org. https://www.mayoclinic.org/tests-procedures/eeg/about/pac-20393875
18. Morley, A. "10-20 System EEG Placement." Www.sleep.pitt.edu, 2016, www.sleep.pitt.edu/wp-content/uploads/2020/03/10-20-system-el.pdf. Accessed 8 Jan. 2024.
19. Murphy, M. P., & LeVine, H. (2010). Alzheimer's Disease and the Amyloid-β Peptide. *Journal of Alzheimer's Disease*, 19(1), 311–323. https://doi.org/10.3233/jad-2010-1221
20. National Health Service. (2019). *Electroencephalogram (EEG)*. NHS. https://www.nhs.uk/conditions/electroencephalogram/
21. Nayak, C. S., & Anilkumar, A. C. (2019). EEG Normal Waveforms. *Nih.gov; StatPearls Publishing*. https://www.ncbi.nlm.nih.gov/books/NBK539805/
22. O'Neil, B., Prichap, L., Roseanne, N., & Chabot, R. (2011). Quantitative Brain Electrical Activity in the Initial Screening of Mild Traumatic Brain Injuries. *Western Journal of Emergency Medicine*, *13*(5), 394–400. https://doi.org/10.5811/westjem.2011.12.6815
23. Paraskevas, G. P., & Kapaki, E. (2021). Cerebrospinal Fluid Biomarkers for Alzheimer's Disease in the Era of Disease-Modifying Treatments. *Brain Sciences*, 11(10), 1258. https://doi.org/10.3390/brainsci11101258
24. Rayi, A., & Murr, N. (2021). Electroencephalogram. *PubMed; StatPearls Publishing*. https://www.ncbi.nlm.nih.gov/books/NBK563295/
25. Scheff, S. W., Price, D. A., Schmitt, F. A., DeKosky, S. T., & Mufson, E. J. (2007). Synaptic alterations in CA1 in mild Alzheimer disease and mild cognitive impairment. *Neurology*, *68*(18), 1501–1508. https://doi.org/10.1212/01.wnl.0000260698.46517.8f
26. Shaw, L. M., Arias, J., Blennow, K., Galasko, D., Molinuevo, J. L., Salloway, S., Schindler, S., Carrillo, M. C., Hendrix, J. A., Ross, A., Illes, J., Ramus, C., & Fifer, S. (2018). Appropriate use criteria for lumbar puncture and cerebrospinal fluid testing in the diagnosis of Alzheimer's disease. *Alzheimer's & Dementia*, 14(11), 1505–1521. https://doi.org/10.1016/j.jalz.2018.07.220
27. Shipley, S. M., Frederick, M. C., Filley, C. M., & Kluger, B. M. (2013). Potential for misdiagnosis in community-acquired PET scans for dementia. *Neurology: Clinical Practice,* 3(4), 305–312. https://doi.org/10.1212/cpj.0b013e318296f2df
28. Smailovic, U., & Jelic, V. (2019). Neurophysiological Markers of Alzheimer's Disease: Quantitative EEG Approach. *Neurology and Therapy*, 8(S2), 37–55. https://doi.org/10.1007/s40120-019-00169-0
29. St, E. K., Frey, L. C., Britton, J. W., Frey, L. C., Hopp, J. L., Pearce Korb, Koubeissi, M. Z., Lievens, W. E., Pestana-Knight, E. M., & St, E. K. (2016). Electroencephalography (EEG): An Introductory Text and

Atlas of Normal and Abnormal Findings in Adults, Children, and Infants [Internet]. *American Epilepsy Society*. https://www.ncbi.nlm.nih.gov/books/NBK390346/

30. Stern. (2002). Simultaneous EEG and fMRI of the alpha rhythm. *NeuroReport*, 2487–2492. https://doi.org/10.1097/01.wnr.0000047685.08940.d0
31. Subramanian, J., Savage, J. C., & Tremblay, M.-È. (2020). Synaptic Loss in Alzheimer's Disease: Mechanistic Insights Provided by Two-Photon in vivo Imaging of Transgenic Mouse Models. *Frontiers in Cellular Neuroscience*, 14. https://doi.org/10.3389/fncel.2020.592607
32. Trzepacz, P. T., Hochstetler, H., Wang, S., Walker, B., & Saykin, A. J. (2015). Relationship between the Montreal Cognitive Assessment and Mini-mental State Examination for assessment of mild cognitive impairment in older adults. *BMC Geriatrics*, 15(1). https://doi.org/10.1186/s12877-015-0103-3
33. Tudor, M., Tudor, L., & Tudor, K. I. (2005). [Hans Berger (1873-1941)--the history of electroencephalography]. *Acta Medica Croatica: Casopis Hravatske Akademije Medicinskih Znanosti*, *59*(4), 307–313. https://pubmed.ncbi.nlm.nih.gov/16334737/
34. Vicchietti, M., Ramos, F. M., Betting, L.E., & Andriana S. L. O. Campanharo. (2023). Computational methods of EEG signals analysis for Alzheimer's disease classification. *Scientific Reports*, 13(1). https://doi.org/10.1038/s41598-023-32664-8
35. Vichianin, Y., Khummongkol, A., Chiewvit, P., Raksthaput, A., Chaichanettee, S., Aoonkaew, N., & Senanarong, V. (2021). *Accuracy of support-vector machines for diagnosis of alzheimer's disease, using volume of* Hojjat Adeli, Samanwoy Ghosh-Dastidar, & Nahid Dadmehr. (2005). Alzheimer's Disease: Models of Computation and Analysis of EEGs. *Clinical Eeg and Neuroscience*, *36*(3), 131–140. https://doi.org/10.1177/155005940503600303
36. Wong, D. F., Maini, A., Rousset, O. G., & Brašić, J. R. (2003). Positron Emission Tomography. *Alcohol Research & Health,* 27(2), 161–173. https://www.ncbi.nlm.nih.gov/pmc/articles/PMC6668888/
37. Xia, W., Zhang, R., Zhang, X., & Usman, M. (2023). A novel method for diagnosing Alzheimer's disease using deep pyramid CNN based on EEG signals. *Heliyon*, *9*(4), e14858. https://doi.org/10.1016/j.heliyon.2023.e14858